



Multi-response optimization of CuZn39Pb3 brass alloy turning by implementing Grey Wolf algorithm

Nikolaos Fountas

School of Pedagogical and Technological Education, Department of Mechanical Engineering Educators, Laboratory of Manufacturing Processes and Machine Tools, ASPETE Campus, GR 14121, N. Heraklion, Greece
fountasnikolaos@hotmail.com

Angelos Koutsomichalis

Hellenic Air-Force Academy, Faculty of Aerospace Studies, Dekelia Air Force Base, GR 19005, Greece
angelos.koutsomichalis@hafa.haf.gr

John D. Kechagias

Technological Educational Institute of Thessaly, Mechanical Engineering Department, TEI Campus, GR 41110, Larissa, Greece
jkechag@teilar.gr

Nikolaos M. Vaxevanidis

School of Pedagogical and Technological Education, Department of Mechanical Engineering Educators, Laboratory of Manufacturing Processes and Machine Tools, ASPETE Campus, GR 14121, N. Heraklion, Greece
vaxer@aspete.gr

ABSTRACT. Machinability of engineering materials is crucial for industrial manufacturing processes since it affects all the essential aspects involved, e.g. workload, resources, surface integrity and part quality. Two basic machinability parameters are the surface roughness, closely associated with the functional and tribological performance of components, and the cutting forces acting on the tool. Knowledge of the cutting forces is needed for estimation of power requirements and for the design of machine tool elements, tool-holders and fixtures, adequately rigid and free from vibration. This work investigates the influence of cutting conditions on machinability indicators such as the main cutting force F_c and surface roughness parameters R_a and R_t when longitudinally turning CuZn39Pb3 brass alloy. Full quadratic regression models were developed to correlate the machining conditions with the imparted machinability characteristics. Further on, an advanced artificial grey wolf optimization algorithm was implemented to optimize the aforementioned responses with great success in finding the final optimal values of the turning parameters.

KEYWORDS. Turning; Surface roughness; Cutting forces; Multi-parameter analysis; Optimization; Grey Wolf algorithm.



Citation: Fountas, N.A., Koutsomichalis, A., Kechagias, J.D., Vaxevanidis, N.M., Multi-response optimization of CuZn39Pb3 brass alloy turning by implementing Grey Wolf algorithm, *Frattura ed Integrità Strutturale*, 50 (2019) 584-594.

Received: 23.01.2019

Accepted: 27.05.2019

Published: 01.10.2019

Copyright: © 2019 This is an open access article under the terms of the CC-BY 4.0, which permits unrestricted use, distribution, and reproduction in any medium, provided the original author and source are credited.



INTRODUCTION

Due to their physical and mechanical properties copper and zinc alloys (brass) possess excellent machinability; high electric as well as thermal conductivity, significant resistance to corrosion and noticeable antibacterial properties. Consequently they are used in several industrial branches such as electronics, sanitary and automotive. Lead (Pb) is a key element added to Brass alloys to facilitate chip breakage, extend tool life and allow for wider applicable ranges of machining parameters [1]. On the other hand, it must be noted that in recent years the use of lead in brass alloys is restricted more and more, due to the legislation on protecting health and environment, since lead is a hazardous heavy metal. Alternatively, numerous studies revealed that adding bismuth, selenium, indium, as well as graphite as substitution for lead improves the machinability of lead-free brasses. However, the manufacturing process of these materials is very complex and cost-intensive. Apart from that, low-leaded binary brass alloys, meeting the future requirements on maximum lead contents of 0.1%-0.25%, have been developed recently. In general, machinability of low-leaded brasses is significantly worse compared to leaded free-brass whilst given their chemical composition and microstructure, different machinability problems arise [2]. For the silicon alloyed materials, i.e. CuZn21Si3P (CW724R), tool wear is to be higher due to a silicon-rich and hard κ -phase in the microstructure. For other low-leaded brasses, such as CuZn42 (CW510L) and CuZn38As (CW511L), the main problems exist due to the formation of long chips and higher thermal as well as mechanical tool load [3]. Additionally, high adhesion tendency may result in chipping of the cutting edge and reduced work piece quality. Kato et al. [4] enhanced the chip evacuation in micro-drilling of CuZn21Si3P by optimizing tool geometry. Klocke et al. [2] and Nobel et al. [3] published approaches to enable high-performance cutting of low-leaded brass alloys. In Ref. [5] Nobel et al. investigates also the chip formation, the flow and its breakage in free orthogonal cutting. Metal cutting operations are widespread in manufacturing industry and the prediction and/or the control of the resulted machinability always is of great importance.

One basic machinability parameter is the surface roughness, as it is closely associated with the quality, reliability and functional performance of components [6,7]. Another one is the cutting force system developed; it is needed for the estimation of power requirements and for the design of machine tool elements, tool-holders and fixtures, adequately rigid and free from vibration. Moreover, the cost of machining is strongly dependent on the rate of material removal, and this cost may be reduced by increasing the cutting speed and/or the feed rate; however, there are restrictions to the speed and feed values above which the life of the tool is shortened excessively. Axis-symmetrical components are primarily manufactured using turning operations. Due to the various factors influencing surface integrity in turning, non-competitive production times as well as poor surface finish may be experienced which in turn degrade functional behavior of turned components [8]. Therefore, as it occurs in any other metal cutting process and any other engineering material, finding the optimal process parameters is of paramount importance [8,9]. Arc-chain surface patterns are quite often in turning, yet; significant deviations may be observed owing to irregular chip formation phenomena such as discontinuous chip, built-up edge, low feeds, chattering and intense tool flank wear. Such occurrences are experienced especially when it comes to productivity or material selection limitations [6].

Manufacturing operations should be performed such that all aspects of design requirements for high performance, aesthetics and functionality are met. Obviously such requirements are directly related to dimensioning and tolerancing as well as surface texture indicators for ensuring longer lifespan for manufactured components and tribological functioning [10]. Despite the fact that arithmetic surface roughness average (R_a) and the maximum height of the profile (R_t) are not able to provide full information about the shape of profile they are two crucial indicators for judging surface finish. Characteristics like inclination and curvature of the surface roughness asperities, “emptiness” or “fullness” of the profile, distribution of the profile material at various heights are registered in the profile shape. The essential tribological aspects (e.g. friction, wear, state of lubrication) are highly dependent on profile shape [7,11-13]. Cutting forces occur when extreme conditions encountered at the tool-workpiece contact [7,14,15]. This interaction can be related to tool wear and failure. As a result tool wear and cutting forces are related to each other. Surface roughness as well as cutting force monitoring is essential for evaluating the performance of machining processes, expand tool life and improve productivity. Nowadays, due to the development of computer technology, finite element and soft computing/artificial intelligence techniques are being used extensively for modeling and optimization of machining processes. Soft computing/ artificial intelligence methods include neural network (NN), fuzzy set theory, genetic algorithm (GA), simulated annealing (SA), ant colony optimization (ACO) and particle swarm optimization (PSO); see Refs. [7,14]. The present study investigates the influence of cutting parameters on machinability indicators such as the main cutting force F_c and surface roughness parameters R_a and R_t when longitudinally turning CuZn39Pb3 brass alloy. Full quadratic regression models were developed to express the correlation of the machining conditions with the imparted machinability characteristics. Further on, an advanced artificial grey wolf optimization algorithm [16] was implemented to optimize successfully the aforementioned responses.



It should be noted that nowadays, due to the increasing trend towards unmanned manufacturing systems, machinability assessment procedures are crucial part in process planning for machining. These procedures are based on a number of either individual or combined machinability criteria such as the tool-life and wear, material removal rate, cutting monitoring of cutting forces and/or power consumption, surface finish and machining accuracy [17]. In particular, for continuous mode machining operations, such as turning, achieving efficient chip breaking is necessary and therefore the chip breakability rating under the selected cutting conditions can be considered as an essential machinability criterion [17-19].

EXPERIMENTAL WORK

The main cutting conditions, rotational speed n , feed rate f and depth were systematically studied by using an L18 mixed-level Taguchi Orthogonal Array for building an experimental design. The scope of the experiment is the investigation of the effect of cutting conditions on surface roughness parameters; R_a and R_t , as well as main cutting force component; F_c , when turning CuZn39Pb3 (CW614N) alloy. The formulation of full quadratic prediction models are also of major concern. A randomized order of executions was followed to eliminate the experimental bias for the results. Table 1 summarizes the turning parameters and their levels.

Parameter	Units	Level 1	Level 2	Level 3
Spindle speed (n)	rpm	800	1600	-
Feed rate (f)	mm/rev	0.10	0.18	0.33
Depth of cut (a)	mm	0.5	1.0	1.5

Table 1: Investigated machining conditions and levels.

Turning experiments were performed on a Colchester Triumph® 2500 conventional lathe. Cylindrical rods of 40 mm in diameter and 150 mm in length were used as the experimental specimens. Regions of cut were determined as 20 mm wide to provide space for the measurements. A SECO® coated tool insert, coded as TNMG 160404 – MF2 with TP 2000 coated grade, was selected as a cutting tool for the series of experiments performed. The tool had a triangular geometry with cutting edge angle, $K_r=55^\circ$. The kinematics of the longitudinal turning process is illustrated in Fig.1a. A 3D cutting force system was considered according to standard theory of oblique cutting; see also Fig.1b. Note that the cutting force is of the most important yet least understood operation parameters of a machining operation. In general, this force is represented by three components, namely, the power component (F_c), the radial component (F_r) and the axial (or feed) component (F_f) as shown in Fig.1b. Of these three components, the greatest, usually, is the power component, which is often called the main cutting force (F_c) [7].

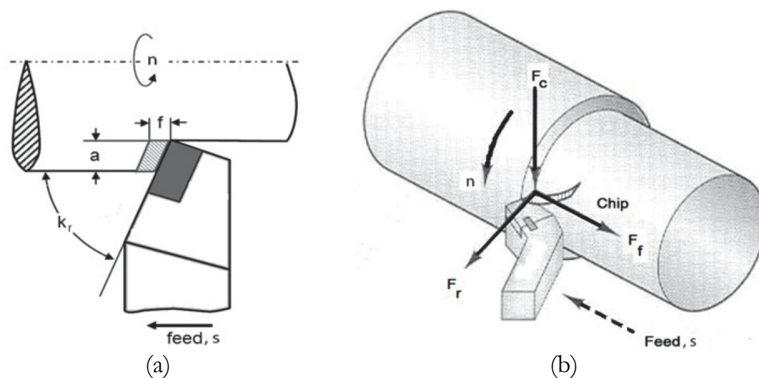


Figure 1: (a) Kinematics of the longitudinal turning process; (b) Three-dimensional cutting force system.

The material under investigation was a CuZn39Pb3 (CW614N-brass 583) brass alloy of 130 HB hardness. Studies concerning the microstructure and machinability of CuZn39Pb3 alloy may be found in [13,20,21]. Surface roughness was evaluated using a Taylor-Hobson® Surtronic 3 profilometer with the Talyprof® software. The cut-off length was selected at 0.8 mm whereas five measurements were taken on every pass at the longitudinal direction. The three-component cutting force

dynamometer Kistler® CH-8408 was used for measuring cutting forces. A typical filtered profile corresponding to a surface roughness measurement is depicted in Fig.2 and an indicative cutting forces measurement graph is shown in Fig.3. Measured values for the objectives Ra, Rt and Fc are tabulated in Table 2 along with the corresponding cutting conditions.

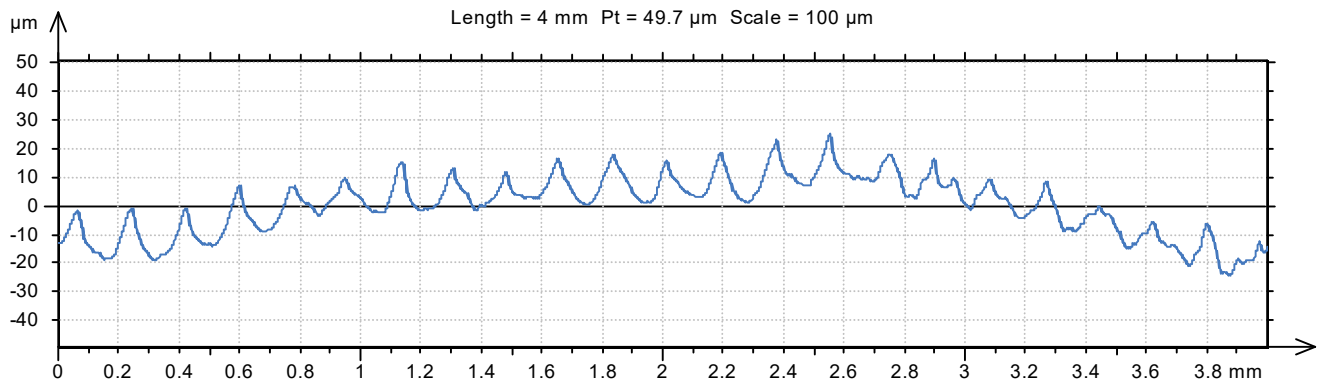


Figure 2: Typical filtered surface roughness profile of a turned brass alloy.

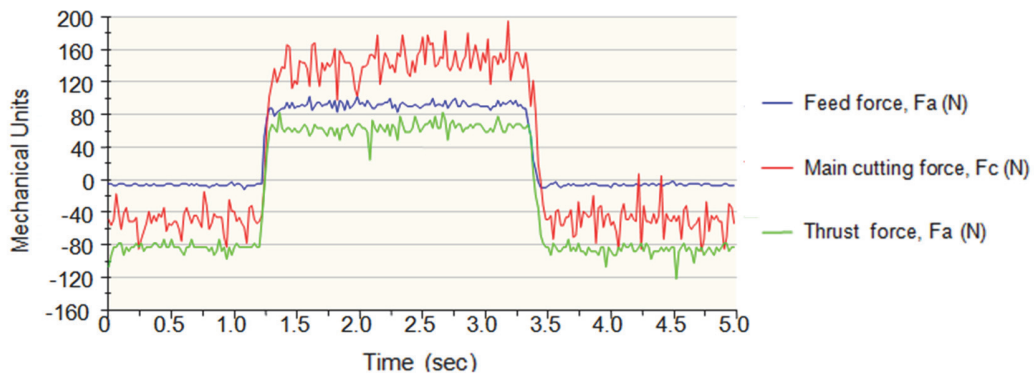


Figure 3: Indicative graph of the cutting forces measurement from a turning experiment.

RESULTS AND DISCUSSION

In the case of steels it was identified [9,22], that surface roughness decreases with increasing cutting speed and decreasing depth of cut and feed rate; such a behavior was not observed for the CuZn39Pb3 brass alloy. During the present series of experiments it is observed that high values for rotational speed in relation to moderate feeds are necessary to minimize surface roughness, whilst combinations of low speeds and low-to-moderate feeds favor the minimization of main cutting force; see Table 2.

These observations are, in general, in agreement with previous reports; see Refs. [2,14]. Fc is reduced under low values for depth of cut and constant rotational speed $n=800$ rpm whilst it increases for $f=0.1$ mm/rev and $f=0.33$ mm/rev. However, a feed rate value $f=0.18$ mm/rev seems to reduce Fc referring to all three levels for depth of cut (Fig.4a). In addition Ra reduces when applying moderate cutting depth levels; i.e., 1.0 mm under constant rotational speed, $n=800$ rpm. A feed rate equal to 0.18 mm/rev reduces Ra under a cutting depth equal to 0.5 mm and 1.0 mm. When applying depth of cut $a=1.0$ mm the increase of Ra is less noticeable under the feed rate level of 0.33 mm/rev. The opposite observation is noticed for Ra when applying a depth of cut equal to 1.5 mm. Ra increases for depth of cut $a=1.5$ mm and feed rate $f=0.1$ mm/rev whilst it reaches its highest value for $f=0.18$ mm/rev (Fig.5a). Rt reduces when applying depth of cut 1.0 mm and 1.5 mm under a feed rate value $f=0.18$ mm yet; a different behavior is noticed when applying a depth of cut equal to 0.5 mm. Rt gradually increases when applying higher values for feed rate under a constant depth of cut equal to 0.5 mm (Fig.6a). For $n=1600$ rpm main cutting force Fc is reduced under the lowest depth of cut as it is expected. Main cutting force seems to increase in general when using high feed rate values however when applying depth of cut equal to 1.0 mm both the second and the third feed rate levels maintain the result of Fc. Main cutting force Fc, reaches its highest value when applying depth of cut equal to 1.5 mm and feed rate equal to 0.33 mm/rev whereas it reaches its lowest value for depth of



cut equal to 0.5 mm and feed rate equal to 0.1 mm/rev (Fig.4b). As opposed to the case of using $n=800$ rpm, depth of cut doesn't seem to significantly affect Ra when applying $n=1600$ rpm. However it seems to slightly increase under higher depth of cut and feed rate values (Fig.5b). As far as Rt is concerned, it takes its lowest value when using the second level of cutting depth which is equal to 1.0 mm and under $f=0.1$ mm/rev (Fig.6b). Nevertheless, switching from $f=0.18$ mm/rev to $f=0.33$ mm/rev an exponential increase to the result of Rt is noticed. By taking into account the levels for rotational speed, $n=800$ rpm and $n=1600$ rpm similar effects are shown for depth of cut $a=0.5$ mm as well as $a=1.0$ mm as opposed to $a=1.5$ mm where different results in terms of the effects are observed, when it comes to Rt. Finally Rt parameter takes its highest value when applying $a=0.5$ mm and $f=0.33$ mm/rev.

Experiment	n (rpm)	f (mm/rev)	a (mm)	Ra (μm)	Rt (μm)	F_c (N)
1	800	0.10	1.5	7.34	37.7	200
2	800	0.10	1.0	4.33	25.6	160
3	800	0.10	0.5	6.02	36.5	090
4	800	0.18	1.5	4.62	25.2	130
5	800	0.18	1.0	4.23	21.1	120
6	800	0.18	0.5	5.52	34.5	080
7	800	0.33	1.5	7.14	33.8	165
8	800	0.33	1.0	8.51	42.7	160
9	800	0.33	0.5	8.02	37.5	100
10	1600	0.10	1.5	1.44	13.2	160
11	1600	0.10	1.0	1.78	11.5	130
12	1600	0.10	0.5	2.03	12.4	085
13	1600	0.18	1.5	4.24	22.2	170
14	1600	0.18	1.0	3.94	19.0	150
15	1600	0.18	0.5	4.00	21.7	100
16	1600	0.33	1.5	5.13	30.7	190
17	1600	0.33	1.0	5.26	26.8	150
18	1600	0.33	0.5	5.28	28.5	110

Table 2: Cutting conditions and measured values of surface roughness parameters and main cutting force.

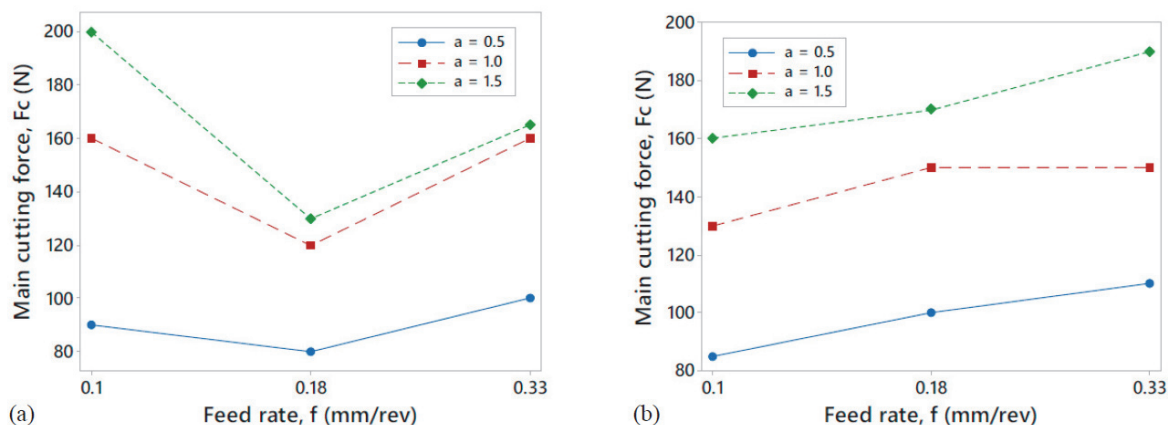


Figure 4: Feed rate effect on main cutting force, F_c : (a) $n=800$ rpm; (b) $n=1600$ rpm.

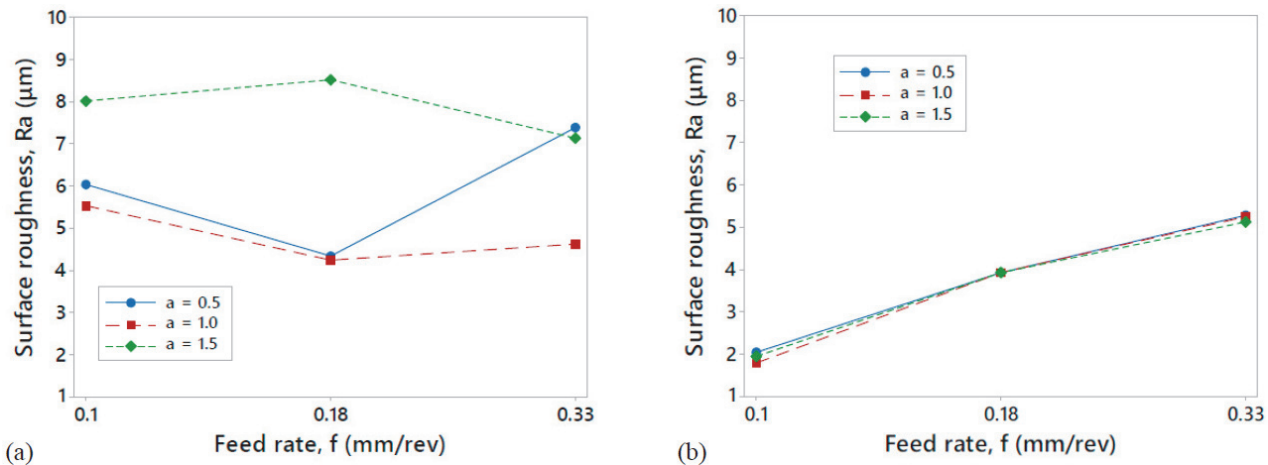


Figure 5: Feed rate effect on mean surface roughness, R_a : (a) $n=800$ rpm; (b) $n=1600$ rpm.

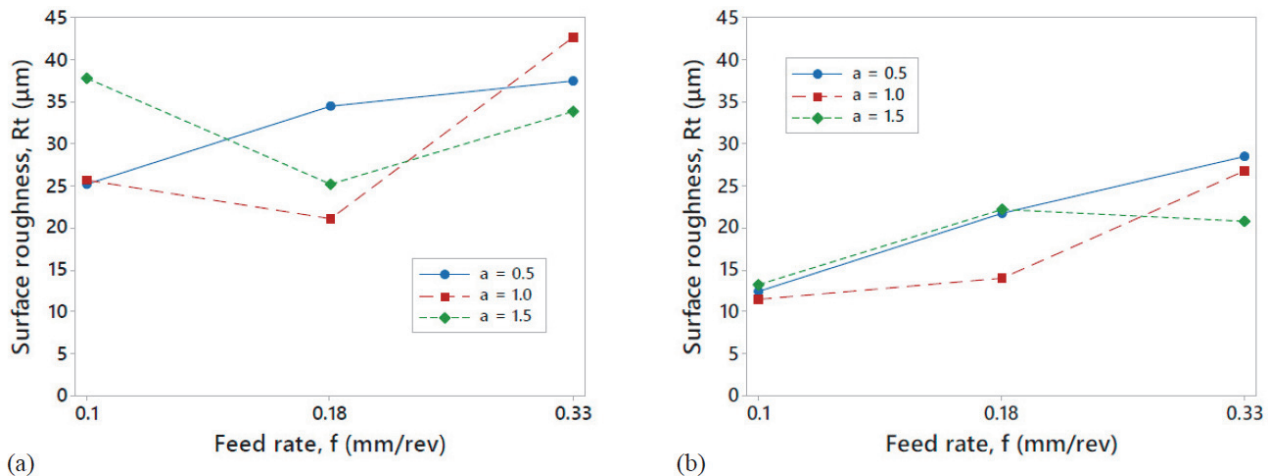


Figure 6: Feed rate effect on maximum surface roughness, R_t : (a) $n=800$ rpm; (b) $n=1600$ rpm.

Statistics and predictive modeling

Regression analysis was applied for developing the second order regression models for responses R_a , R_t and F_c . In order to study the effect of turning parameters on the responses, first order, second order and interactions models among the different levels were considered. The general equation for regression model may be given as:

$$y = b_0 + \sum_{i=1}^n b_i x_i + \sum_{i=1}^n b_{ii} x_i^2 + \sum_i \sum_j b_{ij} x_i x_j \quad (1)$$

In Eq.(1) y is the response; x_i , x_j represent the coded variables corresponding to the rotational speed n (rpm), feed rate f (mm/rev) and depth of cut a (mm) whilst b_i , b_{ii} and b_{ij} are the linear, the quadratic and the interaction terms respectively. The control factors in this relation may change from $i=1$ to n where n is the total number of control factors. By using experiential values of R_a , R_t and F_c , the coefficients for second order regression models have been determined with the help of MINITAB® 17 software by using uncoded units (actual experimental values of process parameters and responses). Final models for R_a , R_t and F_c may be obtained by removing the insignificant terms. The insignificant terms can be removed either by using null hypothesis or by using backward elimination process using p -values of different terms. In this study insignificant terms from the models have been removed by considering p -values. Here, we eliminate the variable (term) with the highest p -value for the test of significance of the variable, conditioned on the p -value being bigger than a predetermined level (0.05 or 95 % confidence level for this case). Next, we fit this model after elimination, and further remove the variable with the highest p -value for the test of significance. The procedure ends when no more variables can be removed from the model. The final models obtained for predicting R_a , R_t and F_c responses are as follows:



$$Ra (\mu\text{m}) = 9.3 - 0.004n - 3.1f - 2.5a + 29.1f^2 + 1.56a^2 + 0.005nf - 0.00002na - 3.5fa \quad (2)$$

$$Rt (\mu\text{m}) = 75.3 - 0.032n - 103f - 35.3a + 210f^2 + 13.5a^2 + 0.051nf + 0.006na - 3.5fa \quad (3)$$

$$Fc (\text{N}) = 69.7 - 0.022n - 612f + 195a + 1283f^2 - 53.4a^2 + 0.135nf - 65fa \quad (4)$$

To test whether the data predicted by regression models are well-fitted or not, the coefficient of determination R^2 has been calculated for each model. These values have been found to be equal to 97.29 %, 96.76 % and 99.44 % for Ra , Rt and Fc respectively. In other words the correlation coefficients for Ra , Rt and Fc are 0.97, 0.96 and 0.99 respectively. Hence, the data predicted by the developed models for each quality characteristic (output) are well-fitted. In order to graphically examine the adequacy of the models, correlation plots were produced. From Fig.7, it is evident that the models developed for fitting the experimental results corresponding to Ra , Rt and Fc are both significant and adequate whilst, simultaneously, they are capable of providing outputs in very good agreement with experimental results.

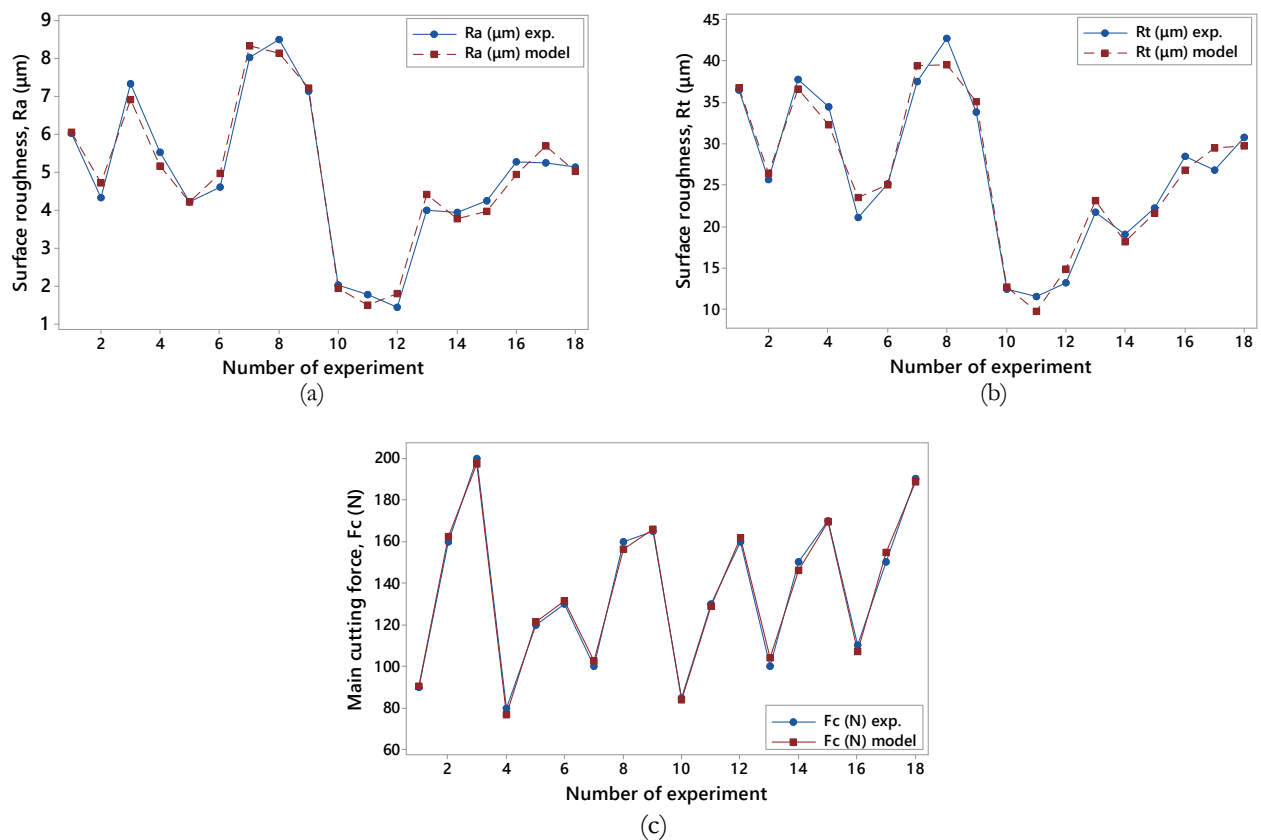


Figure 7: Comparison of experimental and predicted results for: (a) Ra , (b) Rt and (c) Fc .

MULTI-RESPONSE OPTIMIZATION USING THE GREY WOLF ALGORITHM

Meta-heuristic optimization techniques have drawn the researchers' interest over the last two decades. Such techniques are Genetic Algorithms (GAs) [23], Ant Colony Optimization (ACO) [24], and Particle Swarm Optimization (PSO) [25]. In addition to the huge number of theoretical works, such techniques have been applied in various engineering fields. The reason why such algorithms have become very popular in terms of their implementation to engineering problem-solving lies on four main reasons, simplicity; flexibility; derivation-free mechanism; and local optima avoidance. In general, meta-heuristic algorithms are quite simple in their application since they have been mostly inspired by simple concepts. The inspirations mimic physical phenomena like animals' behavior, or evolutionary concepts. This simplicity allows for simulating several natural ideas, proposing novel meta-heuristics, hybridizing two or more meta-heuristics, or



even enhancing current ones. In addition this simplicity contributes to the rapid understanding of metaheuristics for their application to problem-solving. Flexibility deals with the metaheuristics' applicability to the various problems without changing the basic algorithmic infrastructure. Applications of metaheuristics to problems involve only the inputs and outputs of a system. Therefore what needs to be known is how to successfully determine a specific problem to be handled by a metaheuristic. Furthermore the majority of metaheuristics comprise derivation-free utilities. As opposed to gradient-based optimization techniques, metaheuristics optimize problems stochastically. Optimization initializes randomly created candidate solutions, and there is no need to compute derivatives for search spaces to converge to optimal solutions. This makes metaheuristics highly suitable for real-world problems with expensive or unknown derivative information. Finally, metaheuristics exhibit superior abilities to avoid local trapping compared to traditional optimization techniques. This occurs owing to the stochastic nature of metaheuristics allowing them to avoid stagnation in local regions and search the solution space thoroughly. When it comes to real-world problems, solution spaces are usually unknown and quite complex with a vast number of local optima, hence, metaheuristics are suitable modules for optimizing such challenging real-world problems. According to the No-Free Lunch theorem [26] there is no metaheuristic best suited for successfully solving all optimization problems. This implies that a particular metaheuristic may exhibit quite promising results on a set of problems, but the same one might achieve poor performance on a different set of other kinds of problems. Obviously, No-Free Lunch theorem turns this research field to a highly active one where contributions in enhancing current algorithms and/or developing novel ones are published very often.

Fundamental features of the grey wolf algorithm and optimization problem setup

To optimize cutting parameters during turning of CuZn39Pb3 brass alloy, the multi-objective version of grey wolf optimization algorithm was implemented [16]. According to the optimization problem's nature the responses were set for being optimized as follows:

1. Minimization of the arithmetic surface roughness average, R_a ;
2. Minimization of the maximum height of the profile, R_t ;
3. Minimization of the main cutting force, F_c .

The three-objective genetic algorithm optimization method used is a population-based non-dominated intelligent algorithm developed by Mirjalili et al. [16]; following the behavior and social life of grey wolves. This algorithm simulates the haunting hierarchy of wolves towards capturing their prey. The algorithm establishes candidate solutions according to the hierarchy of grey wolves in nature, i.e.; alpha, beta, delta and omega. Mirjalili et al. have properly developed the mathematical relations concerning the unique features of this algorithm based on the physical characteristics of grey wolves. The main stages that grey wolves follow to capture their prey are: 1. Tracking, chasing, and approaching the prey; 2. Pursuing, encircling, and harassing the prey until it stops moving and 3. Attacking the prey. These stages mimic the different intelligent operators an artificial algorithm requires so as to be effective. Hence, attacking a prey technically means the exploitation of the search space whilst searching for prey simulates the exploration of the search space. Of particular interest and practical merit is the C-vector in the grey wolf optimization algorithm. C-vectors suggest random weights for prey so as to stochastically emphasize or partially ignore the effect in defining the Euclidean distance. This contributes to the algorithm's random behavior thus removing the inherent bias of elite solutions and facilitating exploration as well as local optima avoidance. In addition the C-vector can be assumed as the effect of obstacles towards approaching the prey. Thus, depending on the position of a wolf it may randomly give the prey a weight for making it harder to be reached by wolves; or increasing its distance and vice versa. Searching initializes by randomly creating a population of grey wolves (candidate solutions) in the algorithm. Over the course of iterations, alpha, beta, and delta wolves estimate the probable position of the prey. Each candidate solution updates its distance from the prey. The algorithm-specific parameters of the grey wolf algorithm are set accordingly in order to emphasize exploration and exploitation. Finally, the algorithm is terminated once the optimization criteria have been satisfied or the number of generations has been reached.

Optimization results

The results obtained from the grey wolf algorithm for the responses of R_a , R_t and F_c with respect to turning parameters n (rpm), f (mm/rev) and a (mm) are presented in Fig.8 that depicts the non-dominated Pareto optimal solutions obtained. By examining the spread of the non-dominated solutions appeared in the three-objective Pareto front it can be concluded that the non-dominated solutions are concentrated such that all potential values for objectives are obtained. However, since all three optimization criteria are of minimization, it is expected to consider that the non-dominated solutions close to the Pareto front's origin are those of particular benefit. Therefore the non-dominated solutions close to the axes representing the objectives R_a , R_t and F_c are considered as the optimal points for achieving simultaneous optimization, characterized by their parameter values corresponding to the independent variables n (rpm), f (mm/rev) and a (mm).

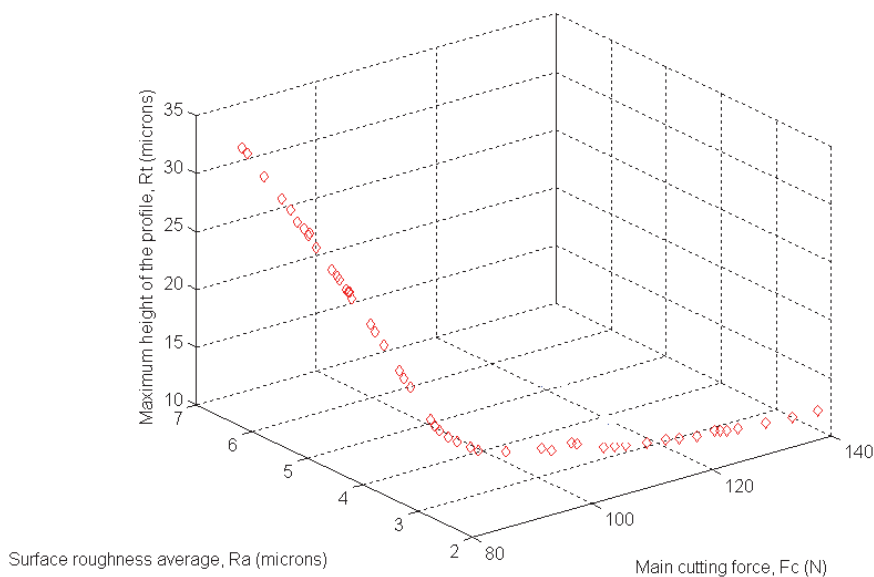


Figure 8: Pareto front of the non-dominated optimal solutions obtained by the multi-objective grey wolf algorithm.

Nevertheless, it is reasonable to argue that the suitability of the different non-dominated solutions provided by the optimization process is to be decided by the process engineer with regard to particular requirements or constraints. This is beneficial to the increase of production rates by reducing machining time as well.

For the purpose of optimizing turning parameters in order to minimize R_a , R_t and F_c a population of 20 grey wolves and a maximum number of 250 iterations were selected. The multi-objective grey wolf algorithm was run several times independently to examine the variability in terms of the obtained results. It was deduced that the algorithm maintains repeatability in converging to the same optimal values despite its stochastic nature. The convergence diagram of the algorithmic evaluations is illustrated in Fig.9. It is shown that the algorithm is capable of obtaining the optimal solution for the three objectives by determining smaller numbers for both candidate solutions and interactions. Apparently the latter depends on the problem's characteristics; optimization trade off (i.e. simultaneous minimization and maximization of several objectives) and settings for algorithm-specific parameters.

The optimal solutions the algorithm obtains refer to alpha, beta and delta wolves holding the best positions in the Pareto front. According to the outputs and the related archive with the resulting costs, the best point of alpha wolf is for $R_a = 3.025 \mu\text{m}$; $R_t = 16.804 \mu\text{m}$ and $F_c = 83.209 \text{ N}$. The values for turning parameters corresponding to these results are 1600 rpm for n ; 0.1184 mm/rev for f and 0.6182 mm for a . The best point of beta wolf is for $R_a = 3.108 \mu\text{m}$; $R_t = 17.180 \mu\text{m}$ and $F_c = 83.153 \text{ N}$. The values for turning parameters corresponding to these results are 1313 rpm for n ; 0.1741 mm/rev for f and 0.5000 mm for a . The best point of delta wolf is for $R_a = 2.966 \mu\text{m}$; $R_t = 16.594 \mu\text{m}$ and $F_c = 83.326 \text{ N}$. The values for

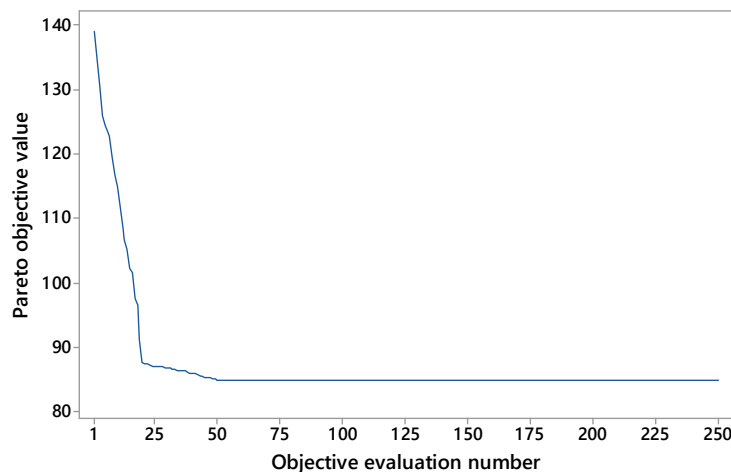


Figure 9: Convergence speed during the algorithmic evaluations performed by the multi-objective grey wolf algorithm.



turning parameters corresponding to these results are 1479 rpm for n ; 0.1709 mm/rev for f and 0.5000 mm for a . It is deduced that the results simultaneously satisfying all three objectives are not necessarily the values of upper or lower points of the problem's intervals. These values for turning parameters occur according the interactions between them. It is also observed that the different solutions prioritize a different hierarchy among the objectives. The best result for R_a comes from the multi-objective solution of the delta wolf which is equal to 2.966 μm whereas the worst value for R_a comes from the multi-objective solution of the beta wolf which is equal to 3.108 μm . The best result for R_t comes from the multi-objective solution of the delta wolf which is equal to 16.594 μm whereas the worst value for R_t comes from the multi-objective solution of the beta wolf which is equal to 17.180 μm . Finally the best best result for F_c comes from the multi-objective solution of the beta wolf which is equal to 83.153 N whereas the worst value for F_c comes from the multi-objective solution of the delta wolf which is equal to 83.326 N. Whether the significance of these small differences among the results is of major or minor importance, it depends on manufacturing specifications and surface finish requirements.

CONCLUSIONS AND FUTURE RESEARCH

In this work an experimental study on machinability parameters in turning of CuZn39Pb3 brass alloy was performed. Machinability was investigated with reference to arithmetic mean surface roughness R_a (μm), maximum height of the profile R_t (μm) and main cutting force F_c (N) which were considered as dependent responses affected by the cutting conditions; rotational speed n (rpm); feed rate f (mm/rev) and depth of cut a (mm). An L18 mixed-level Taguchi orthogonal design of experiments was set to build the design space according to the operational range of cutting conditions as well as their corresponding levels. The results obtained suggest that cutting conditions and their interactions differently affect the responses of R_a , R_t and F_c . Main cutting force is minimized by applying low speeds and moderate feeds whereas roughness parameters R_a and R_t are minimized by using high speeds combined to moderate feeds for a depth of cut equal to 1.0 mm. Full quadratic predictive models were generated via regression analysis and good correlation was achieved between experimental and predicted results for all responses. The resulting models were then considered as the objective functions for solving a multi-response optimization problem for turning of CuZn39Pb3 brass alloy. An advanced multi-objective intelligent algorithm following the behavior and social activity of grey wolves was applied to solve the problem. It was revealed that the algorithm is efficient in its heuristic search during all independent algorithmic runs with emphasis to the final recommended optimal parameters to solve the optimization problem. As a major future perspective the authors currently plan to further investigate soft computing methods and several intelligent algorithms for optimizing the turning of CuZn39Pb3 brass alloy and apply the same methodology to optimize the machining operations such as turning or milling of other engineering materials.

ACKNOWLEDGEMENTS

The authors are grateful to Dr.-Ing. G.A. Pantazopoulos of ELKEME Hellenic Research Centre for Metals s.a for the supply of CuZn39Pb3 brass specimens. N.M. Vaxevanidis wishes to thank the *Special Account for Research of ASPETE* for supporting the presentation of a preliminary version of this work in the “1st International Conference of the GSEMM” through the funding program “Strengthening research of ASPETE faculty members”.

REFERENCES

- [1] Kuyucak, S., Sahoo, M. (1996). A review of the machinability of copper-base alloys, Can. Metall. Quart., 35(1), pp. 1-15.
- [2] Klocke, F., Nobel, C., Veselovac, D. (2016). Influence of tool coating, tool material, and cutting speed on the machinability of low-leaded brass alloys in turning, Mater. Manuf. Process. 31(14), pp. 1895-1903.
- [3] Nobel, C., Klocke, F., Lung, D., Wolf, S. (2014). Machinability enhancement of lead-free brass alloys, Proc. CIRP, 14, pp. 95-100.
- [4] Kato, H., Nakata, S., Ikenaga, N., Sugita, H. (2014). Improvement of chip evacuation in drilling of lead-free brass using micro drill, Int. J. Autom. Technol., 8 (6), pp. 874-879.
- [5] Nobel, C., Hofmann, U., Klocke, F., Veselovac, D. (2015). Experimental investigation of chip formation, flow, and breakage in free orthogonal cutting of copper-zinc alloys, Int. J. Adv. Manuf. Technol., 84(5-8), 1127-1140.



- [6] Petropoulos, G.P., Pandazaras, C.N., Davim, J.P. (2010). Surface texture characterization and evaluation related to machining, In: Surface Integrity in Machining, ed. J.P. Davim, Springer, London, pp. 37-66.
- [7] Vaxevanidis, N.M., Kechagias, J.D., Fountas, N.A., Manolakos, D.E. (2014). Evaluation of machinability in turning of engineering alloys by applying artificial neural networks, Open Construction & Building Technol. J., 8, pp. 389-399.
- [8] Grzesik, W., Kruszynski, B., Ruszaj, A. (2010). Surface integrity of machined surfaces, In: Surface Integrity in Machining, Davim, J.P. (Ed.), Springer, London, pp. 143-179.
- [9] Vaxevanidis, N.M., Galanis, N., Petropoulos, G.P., Karalis, N., Vasilakakos, P., Sideris, J. (2010). Surface roughness analysis in high speed-dry turning of tool steel, Proc. ESDA 2010: 10th Biennial ASME Conference on Engineering Systems Design and Analysis, July 12-14, Istanbul, Turkey.
- [10] Petropoulos, G.P., Pandazaras, C.N., Vaxevanidis, N.M., Antoniadis, A. (2006). Multi-parameter identification and control of turned surface textures, Int. J. Adv. Manuf. Technol. 29, pp. 118-128.
- [11] Petropoulos, G., Pandazaras, C., Vaxevanidis, N.M., Ntziantzias, I., Korlos, A. (2007). Selecting subsets of mutually unrelated ISO 13565-2: 1997 surface roughness parameters in turning operations, Int. J. Comput. Mater. Sci. Surf. Eng., 1(1), pp. 114-128.
- [12] Petropoulos, G., Vaxevanidis, N.M., Pandazaras, C., Koutsomichalis, A. (2009). Postulated models for the fractal dimension of turned metal surfaces, J. Balkan Tribol. Assoc., 15(1), pp. 1-9.
- [13] Toulfatzis, A.I., Pantazopoulos, G.A., Paipetis, A.S. (2014). Fracture behavior and characterization of lead-free brass alloys for machining applications, J. Mater. Eng. Perform., 23, pp. 3193-3206.
- [14] Gaitonde, V.N., Karnik, S.R., Davim, J.P. (2012). Optimal MQL and cutting conditions determination for desired surface roughness in turning of brass using genetic algorithms, Mach. Sci. Technol., 16(2), pp. 304-320.
- [15] Hanief, M., Wani, M.F., Charoo, M.S. (2017). Modeling and prediction of cutting forces during the turning of red brass (C23000) using ANN and regression analysis, Eng. Sci. Technol., 20(3), pp. 1220-1226.
- [16] Mirjalili, S., Mirjalili, S.M., Lewis, A. (2014). Grey Wolf Optimizer, Adv. En. Soft., 69, pp. 46-61.
- [17] Jawahir, I.S. (1988). The chip control factor in machinability assessments: recent trends, J. Mech. Work. Techn., 17, pp. 213-224.
- [18] Jawahir I.S., Van Lutterveld, C.A. (1993). Recent developments in chip control research and applications, Ann. CIRP, 42(2), pp. 659-693.
- [19] Toulfatzis, A.I., Pantazopoulos, G.A., Besseris, G.J., Paipetis, A.S. (2016). Machinability evaluation and screening of leaded and lead-free brasses using a non-linear robust multifactorial profiler, Int. J. Adv. Manuf. Technol., 86(9-12), pp. 3241-3254.
- [20] Pantazopoulos, G. (2002). Leaded brass rods C 38500 for automatic machining operations: a technical report, J. Mater. Eng. Perform. 11(4), pp. 402-407.
- [21] Pantazopoulos, G.A., Toulfatzis, A.I. (2012). Fracture modes and mechanical characteristics of machinable brass rods, Metall., Microstruct., Anal., 1(2), pp. 106-114.
- [22] Galanis, N.I., Manolakos, D.E. (2010). Surface roughness prediction in turning of femoral head, Int. J. Adv. Manuf. Technol., 51(1-4), pp. 79-86.
- [23] Bonabeau, E., Dorigo, M., Theraulaz, G. (1999). Swarm intelligence: from natural to artificial systems: OUP USA.
- [23] Dorigo, M., Birattari, M., Stutzle, T. (2006). Ant colony optimization, Comput. Intell. Magaz., IEEE, 1, pp. 28-39.
- [25] Kennedy, J., Eberhart, R. (1995). Particle swarm optimization in Neural Networks. In: Proceedings, IEEE international conference on Neural Networks ICNN'95, pp. 1942-1948.
- [26] Wolpert, D.H., Macready, W.G. (1997). No free lunch theorems for optimization, IEEE Trans. Evolut. Comput., 1, pp. 67-82.